Structure
Resource

Determining the Oligomeric Structure of Proteorhodopsin by Gd^{3+}-Based Pulsed Dipolar Spectroscopy of Multiple Distances

Devin T. Edwards,[1] Thomas Huber,[2] Sunyia Hussain,[3] Katherine M. Stone,[4] Maia Kinnebrew,[5] Ilia Kaminker,[6] Erez Matalon,[6] Mark S. Sherwin,[1,7] Daniella Goldfarb,[6,*] and Songi Han[4,7,*]
[1]Department of Physics, University of California, Santa Barbara, Santa Barbara, CA 93106, USA
[2]Research School of Chemistry, The Australian National University, Canberra, ACT 0200, Australia
[3]Department of Chemical Engineering, University of California, Santa Barbara, Santa Barbara, CA 93106, USA
[4]Department of Chemistry and Biochemistry, University of California, Santa Barbara, Santa Barbara, CA 93106, USA
[5]College of Creative Studies, University of California, Santa Barbara, Santa Barbara, CA 93106, USA
[6]Department of Chemical Physics, Weizmann Institute of Science, Rehovot, 7610001, Israel
[7]Institute of Terahertz Science and Technology, University of California, Santa Barbara, Santa Barbara, CA 93106, USA
*Correspondence: daniella.goldfarb@weizmann.ac.il (D.G.), songi@chem.ucsb.edu (S.H.)
http://dx.doi.org/10.1016/j.str.2014.09.008

SUMMARY

The structural organization of the functionally relevant, hexameric oligomer of green-absorbing proteorhodopsin (G-PR) was obtained from double electron-electron resonance (DEER) spectroscopy utilizing conventional nitroxide spin labels and recently developed Gd^{3+}-based spin labels. G-PR with nitroxide or Gd^{3+} labels was prepared using cysteine mutations at residues Trp58 and Thr177. By combining reliable measurements of multiple interprotein distances in the G-PR hexamer with computer modeling, we obtained a structural model that agrees with the recent crystal structure of the homologous blue-absorbing PR (B-PR) hexamer. These DEER results provide specific distance information in a membrane-mimetic environment and across loop regions that are unresolved in the crystal structure. In addition, the X-band DEER measurements using nitroxide spin labels suffered from multispin effects that, at times, compromised the detection of next-nearest neighbor distances. Performing measurements at high magnetic fields with Gd^{3+} spin labels increased the sensitivity considerably and alleviated the difficulties caused by multispin interactions.

INTRODUCTION

Membrane proteins are critical for cellular function because they are positioned at the interface of an organelle or the cell with its environment. Despite their immense importance, the structure of membrane proteins remains difficult to characterize because they often resist common experimental approaches (Bill et al., 2011; Carpenter et al., 2008). Although there are ongoing efforts to improve the techniques for characterizing membrane protein structure, another layer of difficulty exists. Many transmembrane proteins are known to oligomerize within the membrane (Fotiadis et al., 2006). Because oligomerization affects protein function—either by enhancing stability or providing specific interactions that tune activity (Cymer and Schneider, 2012)—there is a need to characterize these higher-order structures to deepen our understanding of biological function. However, because of their size and complexity, the structure of membrane protein oligomers remains challenging to capture experimentally.

Here we present an approach, based on pulsed electron paramagnetic resonance (EPR) and Gd^{3+} spin labeling, that promises to be a generally applicable tool to elucidate the structural organization of membrane protein assemblies. We showcase the implementation and strength of this approach by expanding the structural understanding of the green light-absorbing proteorhodopsin (G-PR) oligomer. G-PR is a seven-transmembrane protein encoded by a gene that is widely prevalent in marine bacteria (Béjà et al., 2000, 2001). G-PR likely acts as a light-driven proton pump that enables bacteria to harvest solar energy in a useable form (DeLong and Béjà, 2010), but it displays many unique properties that suggest differences in mechanism or function from the well-studied bacteriorhodopsin proton pump (Hempelmann et al., 2011; Lörinczi et al., 2009; Schäfer et al., 2009). Prior studies have demonstrated that G-PR assembles into hexamers in both 2D crystalline lipids (Klyszejko et al., 2008) and detergent micelle environments (Hoffmann et al., 2010; Stone et al., 2013). Although the functional implications of this assembly are still being investigated, few precise details of the G-PR oligomer structure are currently available. A recent crystal structure (Ran et al., 2013) reveals a doughnut-shaped hexameric assembly for blue-absorbing proteorhodopsin (B-PR), a protein that is homologous to G-PR but differs in its maximum absorption wavelength and photocycle timescale (Hillebrecht et al., 2006; Xi et al., 2008). However, in G-PR hexamers, there has been only a single measurement of a short interprotein distance, which identified a radial orientation of the protein within the hexamer (Stone et al., 2013).

In the past decade, EPR distance measurements have emerged as an important technique to characterize structure in membrane proteins (Altenbach et al., 2008; Georgieva et al., 2013; Hilger et al., 2005; Jeschke, 2013a; Matalon et al., 2013b;

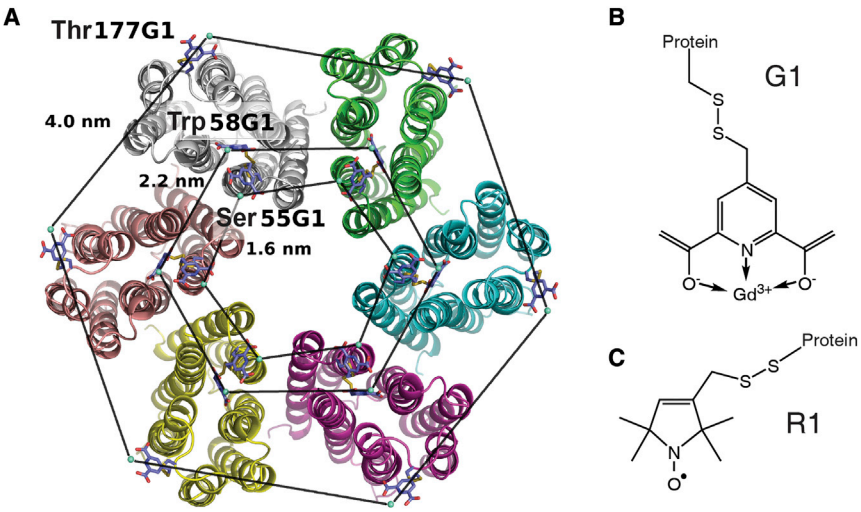

Figure 1. Structure of the G-PR Hexamer and Spin Labels

(A) Model of the structure of the G-PR hexamer based on the B-PR crystal structure (Ran et al., 2013), G-PR monomer structure (Reckel et al., 2011), cw EPR (Stone et al., 2013), and DEER measurements (from this work). The positions of the spin labels used in this study are shown at sites 177 and 58. Additionally, site 55, which was shown to have a short interprotein distance in the cw EPR measurements, is shown for reference.

(B) The 4MMDPA tag with a coordinated Gd^{3+} is shown bound to the cysteine residue of a protein (G1 side chain).

(C) The MTSL spin label is shown bound to the cysteine residue of a protein (R1 side chain).

McHaourab et al., 2011). EPR allows the precise measurement of distances between spin labels attached to proteins or other biomolecules (Berliner et al., 2000). Specifically, double electron-electron resonance (DEER) (Milov et al., 1981; Pannier et al., 2000), a type of pulsed dipolar spectroscopy (PDS), allows measurements of distances and their distributions up to 8 nm using the most common spin labels based on nitroxide radicals (Borbat and Freed, 2013). Spin labels are introduced site-specifically into proteins through site-directed spin labeling techniques (Cornish et al., 1994; Hubbell et al., 2000, 2013) that are compatible with membrane proteins. The sparse distance information obtained with EPR is especially important for studying membrane proteins because their detailed global structure can be difficult to obtain. Even for membrane proteins with known crystal structures, PDS techniques can add significant value by probing structure in diverse lipid and detergent environments (Georgieva et al., 2013; Hänelt et al., 2013; Smirnova et al., 2007) that can influence both membrane protein assembly and function (Gohon and Popot, 2003; Marsh, 2008; Phillips et al., 2009).

It is, however, challenging to fully exploit traditional DEER measurements for structural studies of assemblies comprised of more than two proteins (i.e., oligomers larger than dimers). When more than two nitroxide spins are dipolarly coupled, artifacts in the distance distribution arise because of multispin effects that are not taken into account in the standard DEER data analysis (Jeschke et al., 2009). These artifacts complicate the reliable determination of multiple interspin distances in the same system, reducing the available structural information (Pliotas et al., 2012). Efforts have been made to eliminate multispin effects through experimental (Junk et al., 2011) and data processing (von Hagens et al., 2013) techniques. However, these approaches may not eliminate multispin effects entirely, and some methods require sacrifices to sensitivity.

To overcome these limitations while increasing the sensitivity of the measurements, we complemented standard DEER measurements using nitroxide spin labels with high-field DEER measurements using spin labels based on Gd^{3+} chelates. Recent work in a diverse collection of systems (Kaminker et al., 2012; Lueders et al., 2011; Matalon et al., 2013a; Song et al., 2011; Yulikov et al., 2012) has demonstrated that Gd^{3+} offers many advantages as an alternative spin label for high-field DEER measurements (Goldfarb, 2012, 2014; Potapov et al., 2010b; Raitsimring et al., 2007; Yagi et al., 2011). This manuscript extends the capabilities of Gd^{3+} to include accurately resolving distances between multiple neighboring proteins within a membrane protein oligomer by leveraging the reduction of multispin effects.

We investigate the structure of the G-PR hexamer in a frozen solution of membrane-mimetic, surfactant micelles using two different singly labeled protein mutants. One labeling site is near the oligomer interface and another at the peripheral, third intracellular (E-F) loop, as shown in Figure 1A. DEER measurements using Gd^{3+} labels were performed at the W-band (95 GHz). We also employed traditional nitroxide-based DEER at the X-band (9.5 GHz). As reported previously (Yagi et al., 2011), W-band DEER measurements using the Gd^{3+} feature improved absolute sensitivity compared with X-band measurements with nitroxides. Multispin effects were found to substantially disrupt the distance distributions in measurements with nitroxides, whereas, for measurements with Gd^{3+} labels, they did not exceed the experimental error. As a result, both nearest neighbor and next-nearest neighbor distances were identified reliably in the Gd^{3+}-based DEER measurements. In addition to the methodological advancements presented, these results provide a more complete description of the oligomeric interface and the radial arrangement of G-PR within the hexamer. Using the experimentally determined distances together with computer modeling, we found that the G-PR oligomer structure agreed with the recent crystal structure of the homologous B-PR (Ran et al., 2013), offering a detailed picture of the G-PR hexamer. Importantly, these measurements occur in a functionally active (and potentially tunable) micelle environment and between flexible loop regions that are not resolved by crystallography.

RESULTS

Experimental Approach

Measurements were made on spin-labeled G-PR solubilized in β-dodecylmaltoside (DDM) detergent micelles with the hexamer

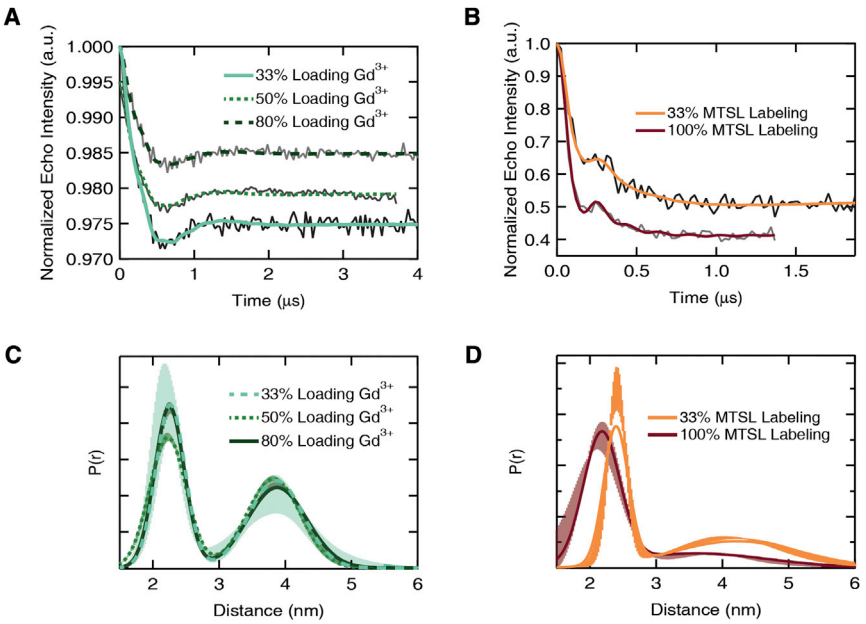

Figure 2. DEER Results for 58G1 and 58R1

(A) Background-corrected, time domain W-band DEER data of the 58G1 G-PR hexamer for 33%, 50%, and 80% Gd^{3+} loading along with the calculated DEER traces. For clarity, the trace from the 50% loading sample has been shifted downward by ~0.005. As described in Supplemental Results, for 58G1 with 33% Gd^{3+} occupancy, a polynomial background was necessary to achieve physical distributions. a.u., arbitrary units.

(B) Background-corrected, time domain X-band DEER data of the 58R1 G-PR hexamer with 33% and 100% nitroxide labeling along with the calculated DEER traces.

(C) The distance distributions for 58G1 (from [A]) obtained utilizing a two-Gaussian distance model. The relative populations of the short and long distance were fixed to be equal. The shaded regions show an estimate of the range of distance distributions that arise from varying the background subtraction. This range is calculated as one SD from the mean distribution determined from a series of possible background subtractions (see Supplemental Results).

(D) The distance distributions for 177R1 (from [B]) obtained utilizing a two-Gaussian distance model. The relative populations of the short and long distance could not be fixed for 100% R1-labeled samples. The relative population of r_1 was 70% for the 100% labeled oligomers. The shaded regions show an estimate of the range of distance distributions that arise from varying the background subtraction. This range is calculated as one SD from the mean distribution determined from a series of possible background subtractions (see Supplemental Results).

See also Figures S1–S4 and Tables S1 and S2.

isolated through size exclusion, fast protein liquid chromatography (Stone et al., 2013). Single cysteine mutations were introduced at residues Trp58 (located at the beginning of the B helix) and Thr177 (located on the loop between the E and F helices). The choice of these sites was guided by their use in a previous study utilizing nitroxide spin labeling to probe the G-PR oligomer interface. In that study, continuous wave (cw) EPR measurements of the nitroxide label at site Ser55 indicated that G-PR organizes radially and that residue 55 is near the center of the oligomer (with a separation of ~1.6 nm between adjacent proteins) (Stone et al., 2013).

This study focuses on determining the interprotein distances for the two sites (58 and 177) that exceed the 2.0 nm ceiling for distance measurements viable by cw EPR lineshape analysis with nitroxides (Jeschke, 2002). This sparse, yet strategically chosen set of interprotein distances can then offer constraints to construct a model of the G-PR organization and the oligomeric interface. Based on previous work (Klyszejko et al., 2008; Stone et al., 2013), we expected site 58 to be located near the center of the hexamer and site 177 at a solvent-exposed, peripheral location of the hexamer (Figure 1A).

The Gd^{3+}-labeled oligomers studied with W-band DEER were prepared by binding the 4-mercaptomethyl-dipicolinic acid (4MMDPA) tag (Su et al., 2008) to the protein, whereas identical G-PR oligomers labeled with S-(2,2,5,5-tetramethyl-2,5-dihydro-1H-pyrrol-3-yl) methyl methanesulfonothioate (MTSL) were prepared and studied with X-band DEER. To distinguish the two labels, we refer to the cysteine-bound MTSL as R1 (as commonly used in the literature; Hubbell et al., 2000) and to the cysteine-bound 4MMDPA with coordinated Gd^{3+} as G1 (Figures 1B and 1C). To control for multispin interactions, spin dilutions were used where only a percentage of the protein (ranging from 33%–100%) is labeled to reduce the average number of spins per hexamer (Junk et al., 2010, 2011).

When statistically labeling a hexamer, multiple interprotein distances are expected to contribute to the measured distance distributions. Each protein in the hexamer has two nearest neighbors (r_1), two next-nearest neighbors (r_2), and the diametrically opposed protein (r_3). For a hexagonal symmetry, these distances should occur with probability ratios of 2:2:1 (i.e., equal probability for the two shorter distances), whereas the interprotein distances should have the ratios r_1:r_2:r_3 = 1:1.73:2.

DEER Results and Observation of Distances between Multiple Neighbors

Background-corrected, time domain DEER traces of 58G1 with 33%, 50%, and 80% Gd^{3+} occupancy are shown in Figure 2A (raw data are shown in Figure S2 [available online], and the Supplemental Results describe the fitting procedure). The sample with 33% Gd^{3+} occupancy had a lower Gd^{3+} concentration (80 μM) than the other samples (150–200 μM), resulting in a lower signal-to-noise ratio (SNR). A distance distribution consisting of the sum of two Gaussian distributions with equal populations (a two-component Gaussian model in DeerAnalysis; Jeschke et al., 2006) provided a very good fit to the data, as shown in Figure 2A. Utilizing a Gaussian distribution for each interprotein distance allows the relative weight of the two distances to be constrained. The choice of a two-Gaussian fit instead of Tikhonov regularization is justified by the consistent observation of two dominant distances in the Tikhonov regularization. These two distances are reproduced by this two-Gaussian component model that better matches the physical organization of the protein hexamer

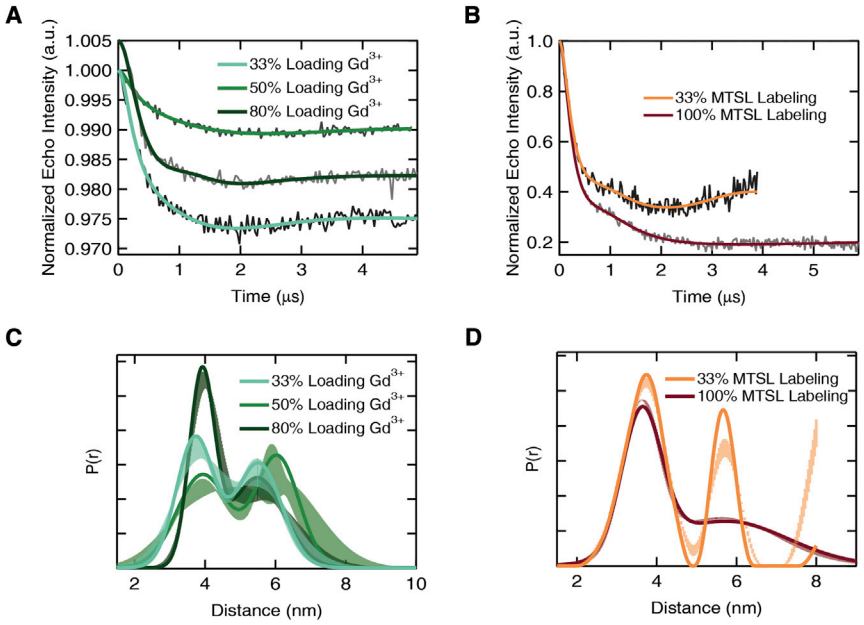

Figure 3. DEER Results for 177G1 and 177R1

(A) Background-corrected, time domain W-band DEER data of the 177G1 G-PR hexamer for 33%, 50%, and 80% Gd^{3+} loading along with the calculated DEER traces. For clarity, the trace for the sample with 80% Gd^{3+} occupancy has been shifted upward by ~0.005.

(B) Background-corrected, time domain X-band DEER data of the 177R1 G-PR hexamer with 33% and 100% nitroxide labeling along with the calculated DEER traces.

(C) The distance distributions for 177G1 (from [A]) obtained utilizing a two-Gaussian distance model. The relative populations of the r_1 and r_2 distance were fixed to be equal. The shaded regions show an estimate of the range of distance distributions that arise from varying the background subtraction. This range is calculated as one SD from the mean distribution determined from a series of possible background subtractions (see Supplemental Results).

(D) The distance distributions for 177R1 (from [B]) obtained utilizing a two-Gaussian distance model. For the 33% labeled 177R1, Tikhonov regularization was first performed and subsequently fit to a two-Gaussian component model (see text and Supplemental Results). The longest peak (~8.0 nm) is beyond the range accessible in our experiments and, therefore, is not considered. The relative populations of the short and long distance were fixed and equal. The shaded regions show an estimate of the range of distance distributions that arise from varying the background subtraction. This range is calculated as one SD from the mean distribution determined from a series of possible background subtractions (see Supplemental Results).

See also Figures S1–S4 and Tables S1 and S2.

from the literature. The resulting distance distributions for 58G1 are shown in Figure 2C. Because the determination of the correct background subtraction can be challenging (Jeschke and Polyhach, 2007), a series of different backgrounds were tested by varying the starting point of the background fit. The distance distribution resulting from the background subtraction that best fit the data is shown as a line in Figure 2C. The shaded regions in the figure indicate the range of distributions determined by averaging all possible background-subtracted spectra that fit the data well (see details in Supplemental Results). The 58G1 samples all give very similar distance distributions with maxima at 2.2 and 3.9 nm. For the sample with 33% Gd^{3+} occupancy, the error due to background subtraction is significantly larger than for other samples (resulting in a much larger range of possible distributions). We attribute this to the lower SNR and associated difficulties in the background decay fit.

The DEER results for 58R1 with 33% and 100% nitroxide labeling are shown in Figures 2B and 2D (raw data are shown in Figure S2). Here the short phase memory time (Figure S3) prevented recording of the DEER traces for long evolution times and, therefore, compromised the SNR. For the 100% nitroxide-labeled samples, we could not fit the data well with two equally weighted Gaussian distributions. Therefore, the relative populations of r_1 and r_2 were also allowed to vary, and the best fit value for the population of r_1 was found to be 70%. The distance distributions (Figure 2D) reveal that the r_2 distance is significantly obscured for both 33% and 100% nitroxide labeling. Furthermore, the distance distributions change significantly as the degree of spin dilution is changed. This is a typical manifestation of multispin effects in DEER results. Multispin interactions have been shown to be more disruptive in high-order oligomers than in lower-order oligomers (Giannoulis et al., 2013), which explains why the effect is so strong in these hexameric assemblies. Nevertheless, the low SNR and short dipolar evolution times can also contribute to these effects. The confidence estimates suggest that the suppression of the r_2 distance is not the result of the background subtraction. Attempts to fit the G1 and R1 data to three Gaussian distributions with fixed relative weights of 2:2:1 did not yield better results than with the simplified assumption of equal populations for the two smaller distances, and r_3 could not be resolved with either of the labels used.

Despite the obscured r_2 distance observed using the R1 labels, the two mean distances of the distance distributions are similar for the R1- and G1-labeled samples at all spin dilutions. The maxima of the best fit distance distributions, averaged over all 58R1 and 58G1 results, are r_1 = 2.3 ± 0.1 nm and r_2 = 3.9 ± 0.2 nm. The average value of the ratio of r_1/r_2 is

$$\kappa_{58} = \frac{r_1}{r_2} = 1.71 \pm 0.03,$$

which is in good agreement with the expected value of 1.73 for a perfect hexamer.

Background-corrected DEER data for 177G1 with 33%, 50%, and 80% Gd^{3+} occupancy are presented in Figure 3A (raw data are shown in Figure S2). The distance distributions obtained using a two-Gaussian component model with equal populations are shown in Figure 3C. Again, the r_1 and r_2 distances are both clearly discernable in the distance distributions for 177G1, although sample-to-sample variations in the width and location of the peak are evident. The r_1 values for 33%, 50%, and 80% Gd^{3+} occupancy are 3.7, 3.9, and 3.9 nm, and the r_2 values are 5.5, 6.0, and 5.5 nm. The variation from background subtraction

contributes some uncertainty to the distributions but cannot entirely account for these discrepancies. We do not attribute the additional variation to multispin effects because multispin effects were not evident for 58G1, which has much shorter interprotein distances. Furthermore, the relative populations of the two distances remained equal, as they should. Instead, we credit the variation in the distance distributions to the relatively broad distributions, the limited dipolar evolution times, and an associated uncertainty in background removal because of the presence of r_3, which is not resolved but may contribute to the tail of the distance distribution. Further discussion regarding the uncertainty in the distance distribution is given in the Supplemental Results.

The results for 177R1 with 33% and 100% labeling are given in Figures 2B and 2D. For 177R1 with 100% nitroxide labeling (Figure 3D), a good fit was obtained using the two-Gaussian component model with equal r_1 and r_2 populations. However, although the r_2 distance is more easily discernable than that for the 58R1 sample, the r_2 distribution is still broadened substantially, causing it to appear weaker than expected. To achieve a physically reasonable distribution for distances in 177R1 with 33% nitroxide labeling, Tikhonov regularization was used to extract the distance distribution. This distribution was then fit to a two-Gaussian component model with equal r_1 and r_2 populations to determine the r_1 and r_2 distances (see Supplemental Results for details). The longest distance (~8 nm) observed in the Tikhonov regularization was discounted because it exceeds the range of distances that can be reliably determined in these measurements. For 33% nitroxide labeling of 177R1, the r_2 distance distribution is not obscured compared with the r_1 distance. We again see significant differences in the distance distributions when varying the degree of nitroxide spin dilution. For both 177R1 samples, the two distances can be well described with equal populations, but the 100% nitroxide-labeled sample still shows a significantly broadened r_2 distance distribution. As with site 58, r_3 is not observed in the measurements of either 177R1 or 177G1. The r_1 and r_2 distances, however, are in good agreement with the 177G1 data.

The average maxima in the distance distributions of 177G1 and 177R1 are r_1 = 3.8 ± 0.1 nm and r_2 = 5.7 ± 0.2 nm. The average value of the r_2/r_1 ratio was $\kappa_{177} = 1.51 \pm 0.06$, significantly lower than the expected $\kappa = 1.73$ that would yield a distance of r_2 = 6.6 nm. This ~0.9 nm difference in the mean r_2 value is outside of the error resulting from background subtraction. The implication of this deviation is discussed later.

If the relative populations of the two distances in the distribution represent physically meaningful results, one expects the r_1 and r_2 distances to appear with equal likelihood for the PR hexamer. For this reason, the two-Gaussian component fits used for the 58G1 and 177G1 data and the majority of the 58R1 and 58G1 samples employed fixed and equal populations of the two distances (Dalmas et al., 2012). However, reasonable fits for the 100% nitroxide-labeled 58R1 data required that the populations be allowed to vary. Generally, R1-labeled samples (Figures 2D and 3D) show a second neighbor distance (r_2) whose distribution is broadened and reduced in intensity, particularly for 58R1. The dominance of the short interprotein distances indicates the presence of multispin effects in nitroxides (Jeschke et al., 2009; Junk et al., 2011). The observation that the artificial exaggeration of the shorter distance is more severe for the closer 58R1 samples than the more distant 177R1 samples is consistent with this concept (Figure 2D versus Figure 3D). Indeed, the strength of the multispin effects in 100% nitroxide-labeled 58R1 explains why the data cannot be successfully described with equal r_1 and r_2 populations. The existence of multispin effects in nitroxides is why the next-nearest neighbor distance is sometimes disregarded in the literature (Pliotas et al., 2012). Interestingly, spin dilutions do not fully eliminate the broadness of the second peak for 58R1, perhaps because of residual multispin effects. Some significant multispins effects may persist in these oligomers with short interprotein distances, given the statistical probability of oligomers containing more than two spin-labeled proteins. This may be exacerbated if the exchange of the protein monomers within the G-PR hexamer-micelle complex is slow, resulting in less than complete mixing of nitroxide-labeled and unlabeled G-PR during sample preparation.

By contrast, when using spin dilutions, the distance distributions for 177G1 and 58G1 change significantly less than with nitroxide-labeled oligomers. Variations that emerge for 177G1 are attributable to experiment factors, including the background subtraction method. Therefore, multispin effects are not observed to significantly affect the DEER results of Gd^{3+}-labeled samples. The overall result is that the distance distributions from G1-labeled oligomers offer a clearer determination of the pair of interprotein distances (r_1 and r_2) without requiring dilution.

The insensitivity of Gd^{3+}–based DEER to multispin effects results from a small modulation depth (λ) of only 1%–3%. The modulation depth is a measure of the probability to flip a spin with the pump pulse of the DEER experiment. It is proportional to the width of the inhomogeneous EPR lineshape and is, therefore, significantly smaller for Gd^{3+} than for nitroxides (Raitsimring et al., 2007). The strength of multispin interactions scales with the modulation depth. Therefore, the three-spin effect will fall off with λ^2, whereas higher-order couplings fall off more rapidly (Jeschke et al., 2009; Junk et al., 2011). Thus, the small λ of Gd^{3+} reduces the distortion of a distance distribution because of the multispin effect.

Data processing techniques exist in the literature to reduce the impact of multispin effects on DEER data (von Hagens et al., 2013). The application of this method to our DEER data (in the DEERAnalysis program; Jeschke, 2013b) for nitroxide-labeled samples was successful in better resolving the r_2 distance (Figure S4 and Supplemental Results). In the case of 100% nitroxide-labeled 58R1, the relative population of the r_1 distance was shifted from 70% to 56% (close to the expected 50%). However, the r_2 distance distribution remained broad, appearing as a shoulder to the dominant r_1 distance distribution. For the case of 100% nitroxide-labeled 177R1, application of the multispin correction shifted the r_2 distances to 6.6 nm, identical to the expected value of 6.6 nm for a perfect hexameric arrangement. The long dipolar evolution time (~5.8 μs) achieved for the 100% nitroxide-labeled 177R1 sample may explain why this longer distance can be observed when multispin effects are eliminated (see Supplemental Results for further discussion). As expected, this specialized processing did not alter the results for Gd^{3+}-labeled proteins, further supporting the observation that multispin effects are reduced in DEER results using Gd^{3+} labels.

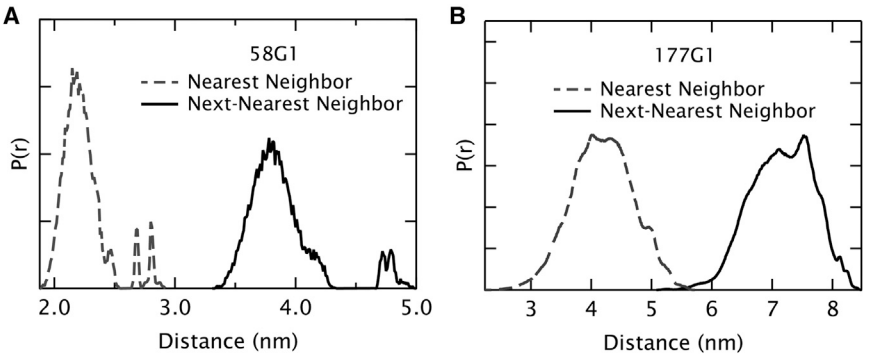

Figure 4. Distance Distributions from the Homology Model

Calculated distance distributions from spin labels in the homology model of G1-labeled G-PR described in the text. Distributions of nearest neighbor Gd^{3+}-Gd^{3+} distances (r_1) and next-nearest neighbors (r_2) are shown.

(A) Distributions for 58G1 using a model with C_6-symmetric labels.

(B) Distributions for 177G1 using a model with nonsymmetric labels.

See also Figure S5.

Distance Limits

The DEER measurements in Figures 2A and 2B show that longer dipolar evolution times (T_{evo}, corresponding to the full length of the time axis) of 3.6–4.0 μs were achieved in 58G1 than the 1.4–1.9 μs obtained for 58R1. Longer dipolar evolution times are extremely advantageous because they allow properties of measured distances (e.g., the mean distance, the width of the distribution) to be confidently reported out to longer distances. An accepted convention (Jeschke, 2013b) is that, for a 2 μs evolution time, the assignment of the mean distance and the distribution width is reliable out to 4 nm and that the mean distance alone is reliable out to 5 nm. These distance limits scale with

$$\left(\frac{T_{evo}}{2\mu s}\right)^{\frac{1}{3}}.$$

Therefore, given the total evolution times for 58R1 ($T_{evo} \sim 1.4$ μs for 100% labeling), we can approximate that the mean distance measured can be trusted out to ~4.4 nm, whereas the width of the distribution is only accurate out to ~3.5 nm. For G-PR labeled at site 58, r_2 ~3.8 nm lies between these two distance limits. By comparison, the >3 μs evolution times achieved in the 58G1 samples allow us to trust the mean distance as well as the width of the distribution out to at least 4.8 nm (and the mean distance alone to at least 6.0 nm). For both 177R1 and 177G1, the evolution times were at least ~4 μs, allowing us to trust the mean distances out to at least 6.2 nm, just beyond the measured r_2 distance of 5.7 nm. However, these dipolar evolution times may still limit the reliable determination of the r_2 distance, resulting in an artificial reduction of r_2 from the expected ~6.6 nm (Supplemental Results). Further details of these distance limits can be found in Supplemental Results, along with Table S1, which details the confidence limits for all samples studied.

The maximum dipolar evolution time is limited by the spin echo decay rate. Direct measurements (Figure S3 and Supplemental Results) show that the echo decays to 10% of its initial intensity within 1.9–4.9 μs in nitroxide-labeled samples (58R1 and 177R1) but within 3.6–4.2 μs for Gd^{3+}-labeled samples (58G1 and 177G1). These results suggest that, for Gd^{3+}-labeled samples, the phase memory time, and, therefore, also the maximum T_{evo}, is less sensitive to the protein environment than for nitroxide labels. Therefore, G1 labels may be more versatile by maintaining evolution times sufficiently long to identify long interspin distances at a wider range of surface-exposed protein sites.

Structural Modeling

To directly relate the distances obtained from the Gd^{3+} spin labels to the structure of the G-PR oligomer, we also calculated the most probable distance distribution between G1 labels utilizing a homology model based on the crystal structure of the B-PR hexamer (Ran et al., 2013) (see Experimental Procedures and Supplemental Results for details). The spin labels were grafted onto the cysteine residue of the labeling sites, and side-chain conformers were generated by randomly varying dihedral angles within ± 10° around preferred rotamer states. Only rotamers that were void of severe steric clashes with the protein were used in further analyses. Because site 177 is located in the E-F loop region of G-PR, which was unresolved in the B-PR crystal structure, the structural model of the E-F loop from a nuclear magnetic resonance (NMR) structure of the G-PR monomer was utilized (Reckel et al., 2011). We hypothesized that labels may arrange cooperatively and assume symmetric orientations. Therefore, for each labeling site, two distance distributions were calculated, assuming either C_6-symmetric labels or uncorrelated, nonsymmetrical labels. Computed spin label distance distributions of 58G1 and 177G1 for r_1 and r_2 are shown in Figure 4 (see Figure S5 for all calculated distributions).

For the structurally buried residue Trp58 (Stone et al., 2013) the distance distribution with symmetrically related labels, having rather narrow distances distributions and maxima at 2.3 nm and 4.0 nm, agrees better with the experimental results than the nonsymmetrical labels. These distances are in excellent agreement with the experimental values of r_1 = 2.3 ± 0.1 nm and r_2 = 3.8 ± 0.2 nm. In addition, the distance distributions are relatively narrow, with a full width at half max (FWHM) of ≈0.3 and ≈0.5 nm for r_1 and r_2, respectively. An increased width of r_2 with respect to r_1 is also consistent with the experimental results obtained with 58G1. The solvent-exposed label at site Thr177 is intrinsically more flexible (Hussain et al., 2013), leading to significantly broader distributions of distances (≈1.5 nm FWHM) with maxima at 4.0 and 7.0 nm. Here the nonsymmetric model showed better agreement with the experimental results than the symmetric one. The short distance is in good agreement with the experimental result of r_1 = 3.8 ± 0.1 nm. However, the next-nearest neighbor distance from this model is ~7.0 nm, which is larger than the experimental value of r_2 = 5.7 ± 0.2 nm.

This experimentally verified, homology-based model is shown in Figure 1A.

The structural model generated from the B-PR hexamer provides an estimate for the furthest interprotein distance (r_3) expected (Figure S5), giving context to the absence of this distance in our measurements. At site 177, the modeling indicates that $r_3 >$ 8 nm, which is generally beyond the range of DEER experiments. In this case, r_3 is probably absorbed in the background decay, adding some uncertainty to the process of background subtraction. However, for site 58, the model suggests $r_3 \sim$4.5–5 nm, which approaches the distance limit that is reliably detectable in these DEER measurements (Table S1). Because we never observe a third distance experimentally, it is likely that the weak dipolar oscillations from the r_3 are either absorbed by the background correction or, more likely, slightly disrupt the r_2 distance distribution.

DISCUSSION

This DEER study improves the previous coarse model of a specific radial orientation of G-PR in a hexameric assembly (Stone et al., 2013) to a more detailed structure that largely agrees with the crystal structure of the B-PR oligomer (Figure 1A). For site 58, the experimental r_1 and r_2 distances both agree well with modeling. However, although the experimental values of r_1 in 177G1 agree well with the model, the experimental r_2 distances are shorter. This may occur because the model does not account for the intrinsic flexibility of the E-F loop site, which appears flexible in the G-PR monomer structure (Reckel et al., 2011). An alternative possibility is that both multispin effects and insufficient dipolar evolution times prevented proper resolution of the r_2 distance out to 6.5 nm (Supplemental Results).

The functional (and possibly structural) distinction between B-PR and G-PR hinges on B-PR existing in marine bacteria deeper in the photic zone of the ocean (Béjà et al., 2001). The tuning of the absorption wavelength is accomplished by replacing the key residue Leu105 in G-PR with glutamine in B-PR (Wang et al., 2003). However, many of the putative oligomeric interface residues (e.g., B helix and flanking loops) are conserved for G-PR and B-PR. Therefore, the agreement between distance measurements in G-PR and the B-PR crystal structure is consistent with the structural similarity of these homologous proteins.

The use of Gd^{3+} spin probes side by side with nitroxide probes demonstrates the strengths of Gd^{3+}-based DEER measurements. As discussed in detail below, DEER measurements at a high magnetic field offer improved sensitivity over measurements of nitroxides at low fields. If required, tuning spin dilution is exceptionally simple with the 4MMDPA Gd^{3+} tag because it involves only the variation of the amount of Gd^{3+} added to the sample without having to alter the protein composition of the sample. Additionally, Gd^{3+} labels appear to preserve long evolution times in a wide variety of labeling locations, offering improved versatility in environmentally heterogeneous biomolecules.

Most critically, Gd^{3+} spin labels are less susceptible to the multispin effects that are highly disruptive for DEER-based structural studies of higher-order oligomers, such as the hexameric G-PR (Giannoulis et al., 2013). Therefore, the scope of DEER measurements of oligomer samples is expanded significantly. Although approximate analytic corrections can be applied in data processing to eliminate multispin effects (von Hagens et al., 2013), they did not fully eliminate the broadness of the r_2 distribution in the 58R1 system (Figure S4). Modifications to the experiment are also possible to reduce multispin effects when using nitroxide probes. For instance, the use of longer microwave pulses reduces λ, which reduces multispin effects. Alternatively, spin dilution, which helped identify the multispin effects in this study, can be employed to curtail multispin effects. However, both of these approaches sacrifice sensitivity and may not eliminate the multispin effect entirely. Additionally, spin dilution of nitroxide-labeled protein complexes requires the production of analog-labeled or wild-type protein samples, and the subsequent physical mixing of the labeled and the unlabeled protein samples may not yield the desired statistical mixtures within the oligomers. Utilizing Gd^{3+} as an alternative spin label makes the sacrifices of signal unnecessary because it inherently reduces multispin effects to allow the robust determination of multiple distances.

In terms of sensitivity, the W-band measurements with Gd^{3+} required an order of magnitude less sample volume than the nitroxide X-band measurements, corresponding to $\sim$0.5 nmol of sample. Alternative Gd^{3+} spin labels based on the 1,4,7,10-tetraazacyclododecane-1,4,7,10-tetraacetic acid chelate offer better sensitivity because of a narrower width of the Gd^{3+} central transition. DEER of samples with spin concentrations as low as 25 μM has been performed on these chelates (Kaminker et al., 2012). Although Gd^{3+}-Gd^{3+} DEER measurements at X-band suffer from low sensitivity and are not recommended, Q-band (34 GHz) measurements are attractive, as reported in several recent studies (Song et al., 2011; Yulikov et al., 2012). For Gd^{3+}, W-band measurements are expected to exhibit a better absolute sensitivity than Q-band measurements. A recent study estimated a factor of about three (Raitsimring et al., 2013). W-band DEER with nitroxides also features high sensitivity, provided that sufficient microwave power is available to generate short enough pulses (Goldfarb et al., 2008; Reginsson et al., 2012). However, there is a high likelihood of orientation selection that prevents a straightforward extraction of the distance distribution when employing nitroxides at the W-band (Polyhach et al., 2007).

Although the molecular-level detail obtained with crystallography or NMR is not rivaled by PDS measurements, the power of these studies lies in the ability to apply them to large and/or complex protein systems and in a variety of sample environments. The spin labeling approach presented here is able to probe a functionally relevant loop region that undergoes a major conformational transformation upon light activation (residue 177 on the E-F loop) (Hussain et al., 2013) but cannot be resolved in most crystal structures given its dynamic nature (Columbus and Hubbell, 2002). Unlike crystallography, PDS also confers the capability to probe distances in a variety of membrane-mimetic surfactant conditions that may alter the oligomeric distribution and interprotein packing (Georgieva et al., 2013; Hänelt et al., 2013). DEER experiments utilizing Gd^{3+}-based spin labels can extend beyond this work, characterizing the hexamer of G-PR to enable structural studies of other membrane protein oligomers.

The application of Gd^{3+}-based PDS in membrane protein assemblies can help fill an important gap in studies of membrane

proteins. The organization of membrane proteins into oligomers is observed in a wide variety of membrane protein systems. For instance, under physiological conditions, many G protein-coupled receptors form assemblies (González-Maeso, 2011), but the structural details of their oligomeric interface remain largely unknown (Ferré and Franco, 2010; Fotiadis et al., 2006). Although oligomerization is thought to tune protein function and/or enhance protein stability (Essen et al., 1998; González-Maeso, 2011), the precise functional role of oligomerization remains debated, especially for α-helical transmembrane proteins such as PR, in which the monomer appears to have all the necessary components for function (Cymer and Schneider, 2012). More generally, the nature of protein-protein interactions and the higher-order structure of multiple proteins in oligomers or during aggregation are important biological factors that can be difficult to quantify. This is particularly true for multimeric transmembrane protein assemblies. Their largely hydrophobic character can be prohibitive for crystallization, and their large size and the necessity for a membrane-mimetic surfactant environment complicates standard NMR analysis. Gd^{3+} labeling can provide the full power and versatility of DEER measurements to study these immensely important oligomeric membrane proteins.

EXPERIMENTAL PROCEDURES

Preparation of Proteorhodopsin Hexamer Samples

The purification and expression of PR followed methods in the literature (Hussain et al., 2013; Stone et al., 2013). The *BAC31A8* G-PR gene (provided by Gregg Whited, Genencor) for green-absorbing proteorhodopsin with a 6× histidine tag at the C terminus and the naturally occurring cysteines (residues 107, 156, and 175) replaced with serines was subcloned into a pTricHis2 plasmid. The cysteine mutations have been shown to not affect overall function (Dioumaev et al., 2003; Krebs et al., 2002; Stone et al., 2013). Further mutagenesis modified the glutamic acid at residue 108 to a glutamine, which extends the M-intermediate state of the photocycle by eliminating a proton acceptor site (Dioumaev et al., 2003; Xi et al., 2008), it but is not expected to affect the oligomer structure. Single cysteine mutations were introduced in the proteins at residues Trp58, and Thr177. Descriptions of the preparation of single cysteine mutants from the plasmid and expression of the protein can be found in Stone et al. (2013).

Purification of G-PR and labeling with nitroxide radicals followed Stone et al. (2013). For labeling using Gd^{3+}, 4MMDPA was used (unmodified from Cedarlane) following previous literature (Potapov et al., 2010b; Su et al., 2008). Both MTSL-labeled and 4MMDPA-labeled G-PR were further purified using size exclusion chromatography with a Sephadex 200 column on a fast protein liquid chromatography instrument (Akta, GE Healthcare). For these experiments, only the fractions identified previously by light scattering as being hexamers in DDM micelles were used for DEER measurements (Stone et al., 2013). The solvent was exchanged for 50 mM Tris buffer made with D_2O containing 0.05 weight percent DDM, and then the solution was concentrated. Gd^{3+} is bound to the 4MMDPA tags through stoichiometric addition of $GdCl_3$ in deuterated buffer following buffer exchange.

Spin-diluted oligomers were generated for both the G1 and R1 samples. Dilutions of 177R1 and 58R1 were prepared by mixing unlabeled G-PR (with no cysteine mutations) with nitroxide-labeled G-PR under conditions that encourage breaking and reforming of interprotein bonds to obtain a statistical dilution (Supplemental Results). Alternatively, for Gd^{3+}-labeled PR samples, the Gd^{3+} label concentration was controlled by maintaining complete 4MMDPA labeling but varying the amount of $GdCl_3$ added to the solution. This dramatically simplifies the measurement of a series of spin dilutions and ensures statistical labeling. The maximum nominal Gd^{3+} loading level utilized was 80% to avoid any chance of free Gd^{3+} in solution (Gordon-Grossman et al., 2011). The samples (both R1 and G1) were diluted to 30:70 d-glycerol:D_2O buffer to ensure the formation of a good glass when frozen by immersion into liquid nitrogen. The estimated spin concentration (as opposed to the protein concentration) was maintained between 150–200 μM for all samples, except for 58G1 with 33% Gd^{3+} occupancy, which was measured at 80 μM.

Optical absorption spectroscopy verified that green light absorption was maintained for the mutated and spin-labeled G-PR variants studied, and only slight shifts in absorption wavelength were observed (Supplemental Results). Furthermore, prior time-resolved optical absorption measurements demonstrate that the main photoactivation properties of slowed photocycle PR are preserved upon mutation and spin labeling as long as green light absorption is present (Hussain et al., 2013). Therefore, we do not expect the overall oligomeric structure studied here to be compromised by either mutation or spin labeling.

X-Band and W-Band DEER Measurements

W-band (95 GHz) pulsed EPR measurements on the Gd^{3+}-labeled protein were carried out at 20 K using a home-built spectrometer (Goldfarb et al., 2008) with 2-3 μl of sample. X-band pulsed EPR (9.5 GHz) measurements were performed at 50 K on a Bruker ELEXSYS E580 spectrometer with 50–60 μl of sample. The "zero" dead time, four-pulse DEER sequence was used for all measurements (Pannier et al., 2000). Phase memory times and echo-detected EPR spectra were measured using a two-pulse spin echo sequence. Further details of the pulse sequences are described in the Supplemental Results, and the spectral locations of the pulses are shown in Figure S1.

The raw DEER data were processed using DEERAnalysis.(Jeschke et al., 2006). Although the Gd^{3+} spin is $S = 7/2$, the analysis method of approximating the Gd^{3+} DEER data using an $S = 1/2$ formalism has been discussed and justified previously (Potapov et al., 2010a, 2010b; Raitsimring et al., 2007).

Structural Model Building

A homology model of G-PR was constructed with the Modeler software (Šali and Blundell, 1993) using the homologous B-PR structure (Protein Data Bank [PDB] ID code 4JQ6; Ran et al., 2013) as a template for the protein core structure. Sequences were aligned using ClustalX (Larkin et al., 2007), and missing loop regions were modeled based on the solution NMR structure of G-PR (PDB ID code 2L6X; Reckel et al., 2011). During model refinement, symmetry restraints were applied to enforce C_6 symmetry of the model. A total of 250 models was computed, and the final model was chosen based on the molpdf score.

To assess the accuracy of the Gd^{3+}-Gd^{3+} DEER distance measurements, we modeled the distance distribution by grafting the Gd^{3+}-4MMDPA tag onto the cysteines at sites 58 and 177 of the G-PR homology model using a procedure described previously (Kaminker et al., 2012). To account for possible inaccuracies in the homology model, van der Waals radii in these calculations were scaled down by one-third for the buried site 58 but assumed the normal values for the solvent-exposed site 177. Further work was done to account for possible effects of symmetry. Details of the modeling are shown in the Supplemental Results and Figure S5.

SUPPLEMENTAL INFORMATION

Supplemental Information includes Supplemental Results, Supplemental Experimental Procedures, five figures, and two tables and can be found with this article online at http://dx.doi.org/10.1016/j.str.2014.09.008.

ACKNOWLEDGMENTS

The authors wish to acknowledge Akiva Feintuch for performing DEER measurements and for assistance with experiments and instrumentation. D.E., S. Han, and M.S. acknowledge funding from the NSF (MRI Grant CHE-0821589 and MCB Grant MCB-1244651) and the W.M. Keck Foundation (Science and Engineering Grant SB-080017). S. Hussain and S. Han acknowledge support from the Institute for Collaborative Biotechnologies through Grant W911NF-09-0001 from the U.S. Army Research Office. This work was also supported by the Israel-USA BSF Science Foundation (D.E., S. Han, M.S., and D.G.). D.G. holds the Erich Klieger professorial chair in Physical Chemistry. Financial support from the Australian Research Council (Grants DP120100561 and FT09917009 to T.H.) is gratefully acknowledged.

Received: April 16, 2014
Revised: August 15, 2014
Accepted: September 4, 2014
Published: October 30, 2014

REFERENCES

Altenbach, C., Kusnetzow, A.K., Ernst, O.P., Hofmann, K.P., and Hubbell, W.L. (2008). High-resolution distance mapping in rhodopsin reveals the pattern of helix movement due to activation. Proc. Natl. Acad. Sci. USA *105*, 7439–7444.

Béjà, O., Aravind, L., Koonin, E.V., Suzuki, M.T., Hadd, A., Nguyen, L.P., Jovanovich, S.B., Gates, C.M., Feldman, R.A., Spudich, J.L., et al. (2000). Bacterial rhodopsin: evidence for a new type of phototrophy in the sea. Science *289*, 1902–1906.

Béjà, O., Spudich, E.N., Spudich, J.L., Leclerc, M., and DeLong, E.F. (2001). Proteorhodopsin phototrophy in the ocean. Nature *411*, 786–789.

Berliner, L.J., Eaton, S.S., and Eaton, G.R., eds. (2000). Distance Measurements in Biological Systems by EPR (Berlin: Springer).

Bill, R.M., Henderson, P.J.F., Iwata, S., Kunji, E.R.S., Michel, H., Neutze, R., Newstead, S., Poolman, B., Tate, C.G., and Vogel, H. (2011). Overcoming barriers to membrane protein structure determination. Nat. Biotechnol. *29*, 335–340.

Borbat, P., and Freed, J. (2013). Pulse Dipolar Electron Spin Resonance: Distance Measurements. (Berlin: Springer), pp. 1–82.

Carpenter, E.P., Beis, K., Cameron, A.D., and Iwata, S. (2008). Overcoming the challenges of membrane protein crystallography. Curr. Opin. Struct. Biol. *18*, 581–586.

Columbus, L., and Hubbell, W.L. (2002). A new spin on protein dynamics. Trends Biochem. Sci. *27*, 288–295.

Cornish, V.W., Benson, D.R., Altenbach, C.A., Hideg, K., Hubbell, W.L., and Schultz, P.G. (1994). Site-specific incorporation of biophysical probes into proteins. Proc. Natl. Acad. Sci. USA *91*, 2910–2914.

Cymer, F., and Schneider, D. (2012). Oligomerization of polytopic α-helical membrane proteins: causes and consequences. Biol. Chem. *393*, 1215–1230.

Dalmas, O., Hyde, H.C., Hulse, R.E., and Perozo, E. (2012). Symmetry-constrained analysis of pulsed double electron-electron resonance (DEER) spectroscopy reveals the dynamic nature of the KcsA activation gate. J. Am. Chem. Soc. *134*, 16360–16369.

DeLong, E.F., and Béjà, O. (2010). The light-driven proton pump proteorhodopsin enhances bacterial survival during tough times. PLoS Biol. *8*, e1000359.

Dioumaev, A.K., Wang, J.M., Bálint, Z., Váró, G., and Lanyi, J.K. (2003). Proton transport by proteorhodopsin requires that the retinal Schiff base counterion Asp-97 be anionic. Biochemistry *42*, 6582–6587.

Essen, L., Siegert, R., Lehmann, W.D., and Oesterhelt, D. (1998). Lipid patches in membrane protein oligomers: crystal structure of the bacteriorhodopsin-lipid complex. Proc. Natl. Acad. Sci. USA *95*, 11673–11678.

Ferré, S., and Franco, R. (2010). Oligomerization of G-protein-coupled receptors: a reality. Curr. Opin. Pharmacol. *10*, 1–5.

Fotiadis, D., Jastrzebska, B., Philippsen, A., Müller, D.J., Palczewski, K., and Engel, A. (2006). Structure of the rhodopsin dimer: a working model for G-protein-coupled receptors. Curr. Opin. Struct. Biol. *16*, 252–259.

Georgieva, E.R., Borbat, P.P., Ginter, C., Freed, J.H., and Boudker, O. (2013). Conformational ensemble of the sodium-coupled aspartate transporter. Nat. Struct. Mol. Biol. *20*, 215–221.

Giannoulis, A., Ward, R., Branigan, E., Naismith, J.H., and Bode, B.E. (2013). PELDOR in rotationally symmetric homo-oligomers. Mol. Phys. *111*, 2845–2854.

Gohon, Y., and Popot, J.-L. (2003). Membrane protein-surfactant complexes. Curr. Opin. Colloid Interface Sci. *8*, 15–22.

Goldfarb, D. (2012). Metal-Based Spin Labeling for Distance Determination. (Berlin: Springer), pp. 1–42.

Goldfarb, D. (2014). Gd3+ spin labeling for distance measurements by pulse EPR spectroscopy. Phys. Chem. Chem. Phys. *16*, 9685–9699.

Goldfarb, D., Lipkin, Y., Potapov, A., Gorodetsky, Y., Epel, B., Raitsimring, A.M., Radoul, M., and Kaminker, I. (2008). HYSCORE and DEER with an upgraded 95GHz pulse EPR spectrometer. J. Magn. Reson. *194*, 8–15.

González-Maeso, J. (2011). GPCR oligomers in pharmacology and signaling. Mol. Brain *4*, 20.

Gordon-Grossman, M., Kaminker, I., Gofman, Y., Shai, Y., and Goldfarb, D. (2011). W-Band pulse EPR distance measurements in peptides using Gd(3+)-dipicolinic acid derivatives as spin labels. Phys. Chem. Chem. Phys. *13*, 10771–10780.

Hänelt, I., Wunnicke, D., Bordignon, E., Steinhoff, H.-J., and Slotboom, D.J. (2013). Conformational heterogeneity of the aspartate transporter Glt(Ph). Nat. Struct. Mol. Biol. *20*, 210–214.

Hempelmann, F., Hölper, S., Verhoefen, M.-K., Woerner, A.C., Köhler, T., Fiedler, S.-A., Pfleger, N., Wachtveitl, J., and Glaubitz, C. (2011). His75-Asp97 cluster in green proteorhodopsin. J. Am. Chem. Soc. *133*, 4645–4654.

Hilger, D., Jung, H., Padan, E., Wegener, C., Vogel, K.-P., Steinhoff, H.-J., and Jeschke, G. (2005). Assessing oligomerization of membrane proteins by four-pulse DEER: pH-dependent dimerization of NhaA Na+/H+ antiporter of E. coli. Biophys. J. *89*, 1328–1338.

Hillebrecht, J.R., Galan, J., Rangarajan, R., Ramos, L., McCleary, K., Ward, D.E., Stuart, J.A., and Birge, R.R. (2006). Structure, function, and wavelength selection in blue-absorbing proteorhodopsin. Biochemistry *45*, 1579–1590.

Hoffmann, J., Aslimovska, L., Bamann, C., Glaubitz, C., Bamberg, E., and Brutschy, B. (2010). Studying the stoichiometries of membrane proteins by mass spectrometry: microbial rhodopsins and a potassium ion channel. Phys. Chem. Chem. Phys. *12*, 3480–3485.

Hubbell, W.L., Cafiso, D.S., and Altenbach, C. (2000). Identifying conformational changes with site-directed spin labeling. Nat. Struct. Biol. *7*, 735–739.

Hubbell, W.L., López, C.J., Altenbach, C., and Yang, Z. (2013). Technological advances in site-directed spin labeling of proteins. Curr. Opin. Struct. Biol. *23*, 725–733.

Hussain, S., Franck, J.M., and Han, S. (2013). Transmembrane protein activation refined by site-specific hydration dynamics. Angew. Chem. Int. Ed. Engl. *52*, 1953–1958.

Jeschke, G. (2002). Determination of the nanostructure of polymer materials by electron paramagnetic resonance spectroscopy. Macromol. Rapid Commun. *23*, 227–246.

Jeschke, G. (2013a). A comparative study of structures and structural transitions of secondary transporters with the LeuT fold. Eur. Biophys. J. *42*, 181–197.

Jeschke, G. (2013b). DeerAnalysis 2013 User Manual. (Zurich: ETH).

Jeschke, G., and Polyhach, Y. (2007). Distance measurements on spin-labelled biomacromolecules by pulsed electron paramagnetic resonance. Phys. Chem. Chem. Phys. *9*, 1895–1910.

Jeschke, G., Chechik, V., Ionita, P., Godt, A., Zimmermann, H., Banham, J., Timmel, C.R., Hilger, D., and Jung, H. (2006). DeerAnalysis2006—a comprehensive software package for analyzing pulsed ELDOR data. Appl. Magn. Reson. *30*, 473–498.

Jeschke, G., Sajid, M., Schulte, M., and Godt, A. (2009). Three-spin correlations in double electron-electron resonance. Phys. Chem. Chem. Phys. *11*, 6580–6591.

Junk, M.J.N., Spiess, H.W., and Hinderberger, D. (2010). The distribution of fatty acids reveals the functional structure of human serum albumin. Angew. Chem. Int. Ed. Engl. *49*, 8755–8759.

Junk, M.J.N., Spiess, H.W., and Hinderberger, D. (2011). DEER in biological multispin-systems: a case study on the fatty acid binding to human serum albumin. J. Magn. Reson. *210*, 210–217.

Kaminker, I., Yagi, H., Huber, T., Feintuch, A., Otting, G., and Goldfarb, D. (2012). Spectroscopic selection of distance measurements in a protein dimer with mixed nitroxide and Gd3+ spin labels. Phys. Chem. Chem. Phys. *14*, 4355–4358.

Klyszejko, A.L., Shastri, S., Mari, S.A., Grubmüller, H., Muller, D.J., and Glaubitz, C. (2008). Folding and assembly of proteorhodopsin. J. Mol. Biol. *376*, 35–41.

Krebs, R.A., Alexiev, U., Partha, R., DeVita, A.M., and Braiman, M.S. (2002). Detection of fast light-activated H+ release and M intermediate formation from proteorhodopsin. BMC Physiol. *2*, 5.

Larkin, M.A., Blackshields, G., Brown, N.P., Chenna, R., McGettigan, P.A., McWilliam, H., Valentin, F., Wallace, I.M., Wilm, A., Lopez, R., et al. (2007). Clustal W and Clustal X version 2.0. Bioinformatics *23*, 2947–2948.

Lörinczi, E., Verhoefen, M.-K., Wachtveitl, J., Woerner, A.C., Glaubitz, C., Engelhard, M., Bamberg, E., and Friedrich, T. (2009). Voltage- and pH-dependent changes in vectoriality of photocurrents mediated by wild-type and mutant proteorhodopsins upon expression in Xenopus oocytes. J. Mol. Biol. *393*, 320–341.

Lueders, P., Jeschke, G., and Yulikov, M. (2011). Double Electron−Electron Resonance Measured Between Gd3+ Ions and Nitroxide Radicals. J. Phys. Chem. Lett.. *2*, 604–609.

Marsh, D. (2008). Protein modulation of lipids, and vice-versa, in membranes. Biochim. Biophys. Acta *1778*, 1545–1575.

Matalon, E., Huber, T., Hagelueken, G., Graham, B., Frydman, V., Feintuch, A., Otting, G., and Goldfarb, D. (2013a). Gadolinium(III) spin labels for high-sensitivity distance measurements in transmembrane helices. Angew. Chem. Int. Ed. Engl. *52*, 11831–11834.

Matalon, E., Kaminker, I., Zimmermann, H., Eisenstein, M., Shai, Y., and Goldfarb, D. (2013b). Topology of the trans-membrane peptide WALP23 in model membranes under negative mismatch conditions. J. Phys. Chem. B *117*, 2280–2293.

McHaourab, H.S., Steed, P.R., and Kazmier, K. (2011). Toward the fourth dimension of membrane protein structure: insight into dynamics from spin-labeling EPR spectroscopy. Structure *19*, 1549–1561.

Milov, A., Salikhov, K., and Shirov, M. (1981). Application of the double resonance method to electron spin echo in a study of the spatial distribution of paramagnetic centers in solids. Sov. Phys. Solid State *23*, 565–569.

Pannier, M., Veit, S., Godt, A., Jeschke, G., and Spiess, H.W. (2000). Dead-time free measurement of dipole-dipole interactions between electron spins. J. Magn. Reson. *142*, 331–340.

Phillips, R., Ursell, T., Wiggins, P., and Sens, P. (2009). Emerging roles for lipids in shaping membrane-protein function. Nature *459*, 379–385.

Pliotas, C., Ward, R., Branigan, E., Rasmussen, A., Hagelueken, G., Huang, H., Black, S.S., Booth, I.R., Schiemann, O., and Naismith, J.H. (2012). Conformational state of the MscS mechanosensitive channel in solution revealed by pulsed electron-electron double resonance (PELDOR) spectroscopy. Proc. Natl. Acad. Sci. USA *109*, E2675–E2682.

Polyhach, Y., Godt, A., Bauer, C., and Jeschke, G. (2007). Spin pair geometry revealed by high-field DEER in the presence of conformational distributions. J. Magn. Reson. *185*, 118–129.

Potapov, A., Song, Y., Meade, T.J., Goldfarb, D., Astashkin, A.V., and Raitsimring, A. (2010a). Distance measurements in model bis-Gd(III) complexes with flexible "bridge". Emulation of biological molecules having flexible structure with Gd(III) labels attached. J. Magn. Reson. *205*, 38–49.

Potapov, A., Yagi, H., Huber, T., Jergic, S., Dixon, N.E., Otting, G., and Goldfarb, D. (2010b). Nanometer-scale distance measurements in proteins using Gd3+ spin labeling. J. Am. Chem. Soc. *132*, 9040–9048.

Raitsimring, A.M., Gunanathan, C., Potapov, A., Efremenko, I., Martin, J.M.L., Milstein, D., and Goldfarb, D. (2007). Gd3+ complexes as potential spin labels for high field pulsed EPR distance measurements. J. Am. Chem. Soc. *129*, 14138–14139.

Raitsimring, A., Astashkin, A.V., Enemark, J.H., Kaminker, I., Goldfarb, D., Walter, E.D., Song, Y., and Meade, T.J. (2013). Optimization of pulsed DEER measurements for Gd-based labels: choice of operational frequencies, pulse durations and positions, and temperature. Appl. Magn. Reson. *44*, 649–670.

Ran, T., Ozorowski, G., Gao, Y., Sineshchekov, O.A., Wang, W., Spudich, J.L., and Luecke, H. (2013). Cross-protomer interaction with the photoactive site in oligomeric proteorhodopsin complexes. Acta Crystallogr. D Biol. Crystallogr. *69*, 1965–1980.

Reckel, S., Gottstein, D., Stehle, J., Löhr, F., Verhoefen, M.-K., Takeda, M., Silvers, R., Kainosho, M., Glaubitz, C., Wachtveitl, J., et al. (2011). Solution NMR structure of proteorhodopsin. Angew. Chem. Int. Ed. Engl. *50*, 11942–11946.

Reginsson, G.W., Hunter, R.I., Cruickshank, P.A.S., Bolton, D.R., Sigurdsson, S.T., Smith, G.M., and Schiemann, O. (2012). W-band PELDOR with 1 kW microwave power: molecular geometry, flexibility and exchange coupling. J. Magn. Reson. *216*, 175–182.

Šali, A., and Blundell, T.L. (1993). Comparative protein modelling by satisfaction of spatial restraints. J. Mol. Biol. *234*, 779–815.

Schäfer, G., Shastri, S., Verhoefen, M.-K., Vogel, V., Glaubitz, C., Wachtveitl, J., and Mäntele, W. (2009). Characterizing the structure and photocycle of PR 2D crystals with CD and FTIR spectroscopy. Photochem. Photobiol. *85*, 529–534.

Smirnova, I., Kasho, V., Choe, J.-Y., Altenbach, C., Hubbell, W.L., and Kaback, H.R. (2007). Sugar binding induces an outward facing conformation of LacY. Proc. Natl. Acad. Sci. USA *104*, 16504–16509.

Song, Y., Meade, T.J., Astashkin, A.V., Klein, E.L., Enemark, J.H., and Raitsimring, A. (2011). Pulsed dipolar spectroscopy distance measurements in biomacromolecules labeled with Gd(III) markers. J. Magn. Reson. *210*, 59–68.

Stone, K.M., Voska, J., Kinnebrew, M., Pavlova, A., Junk, M.J., and Han, S. (2013). Structural insight into proteorhodopsin oligomers. Biophys. J. *104*, 472–481.

Su, X.-C., Man, B., Beeren, S., Liang, H., Simonsen, S., Schmitz, C., Huber, T., Messerle, B.A., and Otting, G. (2008). A dipicolinic acid tag for rigid lanthanide tagging of proteins and paramagnetic NMR spectroscopy. J. Am. Chem. Soc. *130*, 10486–10487.

von Hagens, T., Polyhach, Y., Sajid, M., Godt, A., and Jeschke, G. (2013). Suppression of ghost distances in multiple-spin double electron-electron resonance. Phys. Chem. Chem. Phys. *15*, 5854–5866.

Wang, W.-W., Sineshchekov, O.A., Spudich, E.N., and Spudich, J.L. (2003). Spectroscopic and photochemical characterization of a deep ocean proteorhodopsin. J. Biol. Chem. *278*, 33985–33991.

Xi, B., Tetley, W.C., Marcy, D.L., Zhong, C., Whited, G., Birge, R.R., and Stuart, J.A. (2008). Evaluation of blue and green absorbing proteorhodopsins as holographic materials. J. Phys. Chem. B *112*, 2524–2532.

Yagi, H., Banerjee, D., Graham, B., Huber, T., Goldfarb, D., and Otting, G. (2011). Gadolinium tagging for high-precision measurements of 6 nm distances in protein assemblies by EPR. J. Am. Chem. Soc. *133*, 10418–10421.

Yulikov, M., Lueders, P., Warsi, M.F., Chechik, V., and Jeschke, G. (2012). Distance measurements in Au nanoparticles functionalized with nitroxide radicals and Gd(3+)-DTPA chelate complexes. Phys. Chem. Chem. Phys. *14*, 10732–10746.

